Detection of the Water Reservoir in a Forming Planetary System

Michiel R. Hogerheijde, *et al.*

Science **334**, 338 (2011);
DOI: 10.1126/science.1208931

CORRECTED 23 DECEMBER 2011; SEE LAST PAGE

Detection of the Water Reservoir in a Forming Planetary System

Michiel R. Hogerheijde,[1]* Edwin A. Bergin,[2] Christian Brinch,[1] L. Ilsedore Cleeves,[2] Jeffrey K. J. Fogel,[2] Geoffrey A. Blake,[3] Carsten Dominik,[4] Dariusz C. Lis,[5] Gary Melnick,[6] David Neufeld,[7] Olja Panić,[8] John C. Pearson,[9] Lars Kristensen,[1] Umut A. Yıldız,[1] Ewine F. van Dishoeck[1,10]

Icy bodies may have delivered the oceans to the early Earth, yet little is known about water in the ice-dominated regions of extrasolar planet-forming disks. The Heterodyne Instrument for the Far-Infrared on board the Herschel Space Observatory has detected emission lines from both spin isomers of cold water vapor from the disk around the young star TW Hydrae. This water vapor likely originates from ice-coated solids near the disk surface, hinting at a water ice reservoir equivalent to several thousand Earth oceans in mass. The water's ortho-to-para ratio falls well below that of solar system comets, suggesting that comets contain heterogeneous ice mixtures collected across the entire solar nebula during the early stages of planetary birth.

Water in the solar nebula is thought to have been frozen out onto dust grains outside ~3 astronomical units (AU) (*1*, *2*). Stored in icy bodies, this water provided a reservoir for impact delivery of oceans to the Earth (*3*). In planet-forming disks, water vapor is thought to be abundant only in the hot (>250 K) inner regions, where ice sublimates and gas-phase chemistry locks up all oxygen in H_2O. Emission from hot (>250 K) water has been detected from several disks around young stars (*4*, *5*). In the cold (~20 K) outer disk, water vapor freezes out, evidenced by spectral features of water ice in a few disks (*6*, *7*). However, (inter)stellar ultraviolet radiation penetrating the upper disk layers desorbs a small fraction of water ice molecules back into the gas phase (*8*), suggesting that cold (<100 K) water vapor exists throughout the radial extent of the disk. The detection of this water vapor would signal the presence of a hidden ice reservoir.

We report detection of ground-state rotational emission lines of both spin isomers of water ($J_{K_AK_C}$ 1_{10}-1_{01} from ortho-H_2O and 1_{11}-0_{00} from para-H_2O) from the disk around the pre–main-sequence star TW Hydrae (TW Hya) using the Heterodyne Instrument for the Far-Infrared (HIFI) spectrometer (*9*) on board the Herschel Space Observatory (*10*) (Fig. 1) (*11*, *12*). TW Hya is a 0.6 $M_\odot$ (solar mass), 10-million-year-old T Tauri star (*13*) 53.7 ± 6.2 pc away from Earth. Its 196-AU-radius disk is the closest protoplanetary disk to Earth with strong gas emission lines. The disk's mass is estimated at 2×10^{-4} to 6×10^{-4} $M_\odot$ in dust and, using different tracers and assumptions, between 4×10^{-5} and 0.06 $M_\odot$ in gas (*14*–*16*). The velocity widths of the H_2O lines (0.96 to 1.17 km s^{-1}) (table S1) exceed by ~40% those of cold CO (*14*). These correspond to CO emission from the full 196-AU-radius rotating disk inclined at ~7° with only little (<65 m s^{-1}) turbulence (*17*). The wider H_2O lines suggest that the water emission extends to ~115 AU, where the gas orbits the star at higher velocities compared with 196 AU.

To quantify the amount of water vapor traced by the detected lines, we performed detailed simulations of the water chemistry and line formation using a realistic disk model matching previous observations (*12*, *18*). We adopted a conservatively low dust mass of 1.9×10^{-4} $M_\odot$ and, using a standard gas-to-dust mass ratio of 100, a gas mass of 1.9×10^{-2} $M_\odot$. We explored the effects of much lower gas-to-dust ratios. We followed the penetration of the stellar ultraviolet and x-ray radiation into the disk; calculated the resulting photodesorption of water and ensuing gas-phase chemistry, including photodissociation; and solved the statistical-equilibrium excitation and line formation. The balance of photodesorption of water ice and photodissociation of water vapor results in an equilibrium column of water H_2O vapor throughout the disk (Fig. 2). Consistent with other studies (*19*), we find a layer of maximum water vapor abundance of 0.5×10^{-7} to 2×10^{-7} relative to H_2 at an intermediate height in the disk. Above this layer, water is photodissociated; below it, little photodesorption occurs and water is frozen out, with an ice abundance, set by available oxygen, of 10^{-4} relative to H_2.

In our model, the 100- to 196-AU region dominates the line emission, which exceeds observations in strength by factors of 5.3 ± 0.2 for H_2O 1_{10}-1_{01} and 3.3 ± 0.2 for H_2O 1_{11}-0_{00}. A lower gas mass does not decrease the line intensities, if we assume that the water ice, from

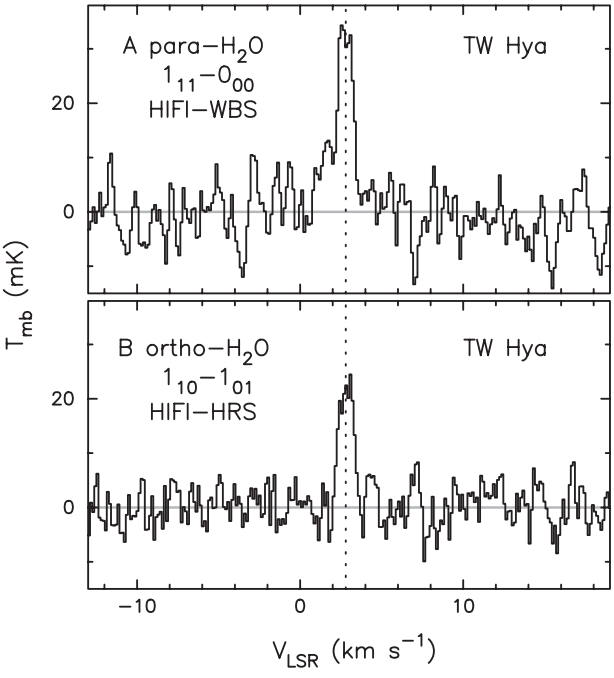

Fig. 1. Spectra of para-H_2O 1_{11}-0_{00} (**A**) and ortho-H_2O 1_{10}-1_{01} (**B**) obtained with HIFI on the Herschel Space Observatory toward the protoplanetary disk around TW Hya after subtraction of the continuum emission. The vertical dotted lines show the system's velocity of +2.8 km s^{-1} relative to the Sun's local environment (local standard of rest).

[1]Leiden Observatory, Leiden University, Post Office Box 9513, 2300 RA Leiden, Netherlands. [2]Department of Astronomy, University of Michigan, Ann Arbor, MI 48109, USA. [3]Division of Geological and Planetary Sciences, California Institute of Technology, Pasadena, CA 91125, USA. [4]Astronomical Institute Anton Pannekoek, University of Amsterdam, 1098 XH Amsterdam, Netherlands. [5]Division of Physics, Mathematics, and Astronomy, California Institute of Technology, Pasadena, CA 91125, USA. [6]Harvard-Smithsonian Center for Astrophysics, Cambridge, MA 02138, USA. [7]Department of Physics and Astronomy, Johns Hopkins University, Baltimore, MD 21218, USA. [8]European Southern Observatory, 85748 Garching, Germany. [9]Jet Propulsion Laboratory, California Institute of Technology, Pasadena, CA 91109, USA. [10]Max-Planck-Institut für Extraterrestrische Physik, 85748 Garching, Germany.

*To whom correspondence should be addressed. E-mail: michiel@strw.leidenuniv.nl

which the water vapor derives, formed early in the disk's evolution, before substantial gas loss occurred, and remains frozen on grains. The most plausible explanation involves a difference in the relative location of small, bare grains regulating the ultraviolet radiative transport and larger, ice-carrying grains. Differential settling of large grains relative to small grains moves much of the ice reservoir below the reach of the ultraviolet radiation, resulting in less water vapor and weaker lines. Our model matches the observations if only 12% of the original ice content remains above this line (*20*). A radially increasing degree of settling of icy grains explains the observed H_2O line widths.

The detected water vapor, resulting from photodesorption, implies an ice reservoir in the giant planet formation zone and beyond. In our simulations, the 7.3×10^{24} g of detected water vapor (equivalent to 0.005 times the mass of Earth's oceans) originate from a total ice reservoir of 9×10^{27} g (or several thousands of Earth's oceans) throughout the disk. The size of this reservoir is tied to the dust mass contained in the disk, for which we adopt a conservatively low value. Although the ice reservoir is only observed indirectly, no known mechanism can remove it from the regions probed by Herschel. Any smaller ice reservoir implies the corresponding absence of elemental oxygen that efficiently reforms water ice on the grains.

The detection of both spin isomers of water vapor allows its ortho-to-para ratio (OPR) to be derived, because our simulations indicate that the lines are optically thin. An OPR of 0.77 ± 0.07 matches our observations (*12*). This value is much lower than the OPR range of 2 to 3 observed for solar system comets (*21*). It is common practice to associate the OPR with a spin temperature T_{spin} at which a Boltzmann distribution reproduces the ratio of spin isomers. Our derived OPR corresponds to $T_{spin} = 13.5 \pm 0.5$ K, whereas the range for solar system comets yields a T_{spin} of >20 K.

Radiative conversion between spin isomers is not allowed in the gas phase, preserving the OPR for long time scales. Gas-phase formation of water occurs through exothermic reactions leading to an OPR of 3. On grains, water forms and survives at low temperatures, and it is tempting to equate T_{spin} with the grain temperature. However, the energetics of water formation and ortho-to-para exchange on grains are poorly understood (*22*), and the water OPR may be changed by photodesorption. This process starts by dissociating water to H and OH in the ice and continues with the energetic H kicking out a neighboring H_2O molecule from the ice matrix or with the H and OH recombining in the ice to form H_2O with sufficient internal energy to sublimate (*23*). The latter route drives the OPR to at least unity, implying an even lower original ice OPR, to yield a resulting OPR of 0.77. Cometary volatiles are released through thermal sublimation, and their measured OPRs are interpreted to reflect the OPR of their ice constituents. Equating T_{spin} with the physical temperature of the grain on which the ice formed is supported by the similarity of measured T_{spin} of NH_3 and H_2O in several individual solar system comets (*24*).

Solar system comets consist of a heterogeneous mixture of ices and solids, likely assembled in the giant planet formation zone by mixing local material with material that drifted in from larger radii (*25*). Our water vapor observations probe cold, ice-coated precometary grains residing beyond >50 AU, representing the bulk of the latter material. The presence in comets of crystalline silicates, requiring formation temperatures >800 K (*26*), together with CO and H_2O ices that condense at 20 to 100 K, argues for transport of hot material from near the star to the icy outer regions of the solar nebula (*27*). Provided that spin temperatures reflect formation histories, the different T_{spin} inferred for the water ice in TW Hya (<13 K) and solar system comets (>20 K) indicates a similar mixing of volatiles throughout the entire solar nebula, blending water formed at >50 K and an OPR of 3 with water formed at 10 to 20 K and an OPR < 1 probed by our observations. In this case, the range of T_{spin} values of the cometary inventory reflects the stochastic nature of transport and mixing.

Our Herschel detection of cold water vapor in the outer disk of TW Hya demonstrates the presence of a considerable reservoir of water ice in this protoplanetary disk, sufficient to form several thousand Earth oceans' worth of icy bodies. Our observations only directly trace the tip of the iceberg of 0.005 Earth oceans in the form of water vapor.

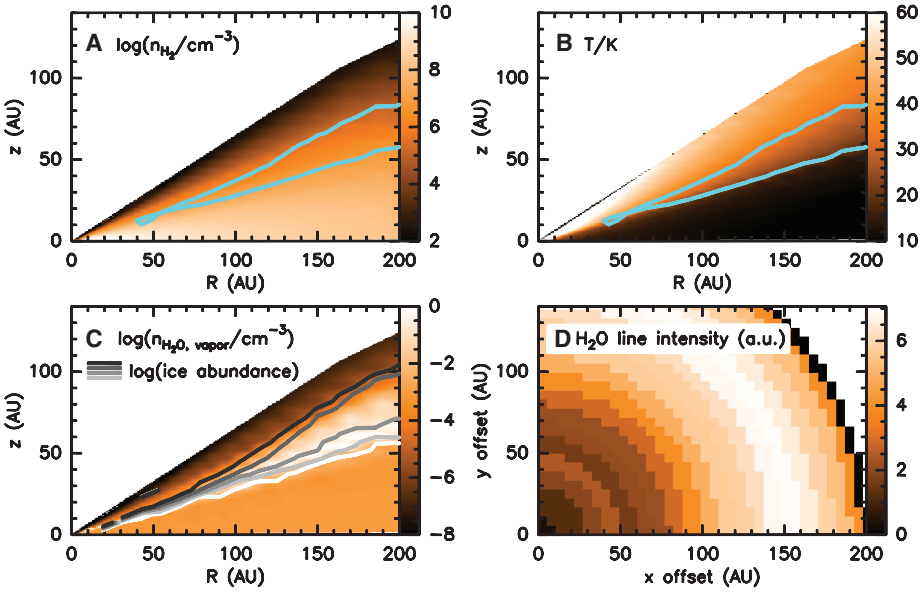

Fig. 2. Adopted model for the TW Hya protoplanetary disk. (**A**) H_2 number density, (**B**) dust temperature, (**C**) the number density of water vapor molecules and contours of volume-averaged water ice abundance decreasing from white to black as 2×10^{-4}, 2×10^{-5}, 2×10^{-6}, 2×10^{-7}, and 2×10^{-8}, relative to H_2, and (**D**) one quadrant of the resulting water emission line intensity from the near face-on disk, in arbitrary units. In (A) and (B), the blue contour delineates the layer of maximum water vapor abundance.

References and Notes

1. One astronomical unit (AU) is the mean distance between Earth and the Sun of 1.49598×10^{11} m.
2. C. Hayashi, *Prog. Theor. Phys.* **70** (suppl.), 35 (1981).
3. T. Matsui, Y. Abe, *Nature* **322**, 526 (1986).
4. K. M. Pontoppidan, C. Salyk, G. A. Blake, H. U. Käufl, *Astrophys. J.* **722**, L173 (2010).
5. J. S. Carr, J. R. Najita, *Astrophys. J.* **733**, 102 (2011).
6. H. Terada *et al.*, *Astrophys. J.* **667**, 303 (2007).
7. M. Honda *et al.*, *Astrophys. J.* **690**, L110 (2009).
8. C. Dominik, C. Ceccarelli, D. Hollenbach, M. Kaufman, *Astrophys. J.* **635**, L85 (2005).
9. T. de Graauw *et al.*, *Astron. Astrophys.* **518**, L6 (2010).
10. G. L. Pilbratt *et al.*, *Astron. Astrophys.* **518**, L1 (2010).
11. Water in Earth's atmosphere obstructs ground-based detection of cold water vapor in planet-forming disks. Although Herschel cannot spatially resolve even the closest disk in water ground-state emission lines, HIFI spectrally resolves the H_2O line profiles. Comparison with previous spectrally and spatially resolved observations of CO confirms the disk origin of the H_2O lines.
12. Materials and methods are available as supporting material on *Science* Online.
13. R. A. Webb *et al.*, *Astrophys. J.* **512**, L63 (1999).
14. J. H. Kastner, B. Zuckerman, D. A. Weintraub, T. Forveille, *Science* **277**, 67 (1997).
15. N. Calvet *et al.*, *Astrophys. J.* **568**, 1008 (2002).
16. U. Gorti, D. Hollenbach, J. Najita, I. Pascucci, *Astrophys. J.* **735**, 90 (2011).
17. A. M. Hughes, D. J. Wilner, S. M. Andrews, C. Qi, M. R. Hogerheijde, *Astrophys. J.* **727**, 85 (2011).
18. W. Thi *et al.*, *Astron. Astrophys.* **518**, L125 (2010).
19. P. Woitke, W. Thi, I. Kamp, M. R. Hogerheijde, *Astron. Astrophys.* **501**, L5 (2009).
20. R. Meijerink, K. M. Pontoppidan, G. A. Blake, D. R. Poelman, C. P. Dullemond, *Astrophys. J.* **704**, 1471 (2009).

21. B. P. Bonev *et al.*, *Astrophys. J.* **661**, L97 (2007).
22. H.-H. Limbach *et al.*, *ChemPhysChem* **7**, 551 (2006).
23. S. Andersson, E. F. van Dishoeck, *Astron. Astrophys.* **491**, 907 (2008).
24. Y. Shinnaka *et al.*, *Astrophys. J.* **729**, 81 (2011).
25. S. J. Weidenschilling, *Mon. Not. R. Astron. Soc.* **180**, 57 (1977).
26. S. A. Sandford *et al.*, *Science* **314**, 1720 (2006).
27. D. H. Wooden, *Space Sci. Rev.* **138**, 75 (2008).

Acknowledgments: Herschel is a European Space Agency space observatory with science instruments provided by European-led principal investigator consortia and with important participation from NASA. This work was partially supported by Nederlandse Organisatie voor Wetenschappelijk Onderzoek grant 639.042.404, NSF grant 0707777, and, as part of the NASA Herschel HIFI guaranteed time program, NASA. The data presented here are archived at the Herschel Science Archive, http://archives.esac.esa.int/hda/ui, under OBSID 1342198337 and 1342201585.

Supporting Online Material
www.sciencemag.org/cgi/content/full/334/6054/338/DC1
Materials and Methods
Table S1
References (*28*–*39*)

25 May 2011; accepted 20 September 2011
10.1126/science.1208931

Supramolecular Linear Heterojunction Composed of Graphite-Like Semiconducting Nanotubular Segments

Wei Zhang,[1,2] Wusong Jin,[3] Takanori Fukushima,[1,4]* Akinori Saeki,[5] Shu Seki,[5] Takuzo Aida[1,2]*

One-dimensionally connected organic nanostructures with dissimilar semiconducting properties are expected to provide a reliable platform in understanding the behaviors of photocarriers, which are important for the development of efficient photon-to-electrical energy conversion systems. Although bottom-up supramolecular approaches are considered promising for the realization of such nanoscale heterojunctions, the dynamic nature of molecular assembly is problematic. We report a semiconducting nanoscale organic heterojunction, demonstrated by stepwise nanotubular coassembly of two strategically designed molecular graphenes. The dissimilar nanotubular segments, thus connected noncovalently, were electronically communicable with one another over the heterojunction interface and displayed characteristic excitation energy transfer and charge transport properties not present in a mixture of the corresponding homotropically assembled nanotubes.

Heterojunctions, occurring between two dissimilar semiconducting materials, are expected to provide peculiar electronic properties that are hard to realize by homojunctions. Heterojunctions of varying dimensions are readily fabricated from inorganic semiconductors and lead to many applications, including solid-state lasers, diodes, solar cells, and transistors (*1*–*6*). Organic heterojunctions are of importance in the development of organic thin-film solar cells (*7*, *8*). However, most that have been studied are so-called bulk heterojunctions, which are formed only coincidentally from donor/acceptor mixtures upon phase separation (*9*–*12*). Although bottom-up supramolecular approaches (*13*, *14*) are a potent tool for the formation of organic heterojunctions, such studies have just started with molecularly engineered donor/acceptor couples (*15*–*19*). From a fundamental viewpoint, one challenge would be to tailor a linear organic heterojunction at the nanoscale by joining together dissimilar semiconducting one-dimensional molecular objects, because one has to overcome the essential problem arising from the dynamic nature of molecular assembly (*13*, *14*, *20*–*24*).

We reported that a Gemini-shaped hexa-*peri*-hexabenzocoronene (HBC) derivative, bearing two triethylene glycol-appended phenyl groups on one side of the HBC core and dodecyl side chains on the other, self-assembles into a semiconducting nanotube with inner and outer diameters of 14 and 20 nm, respectively (*25*, *26*). A recent structural analysis using a synchrotron x-ray diffraction technique revealed that the nanotube is composed of a graphite-like bilayer wall consisting of helically twisted columnar arrays of π-stacked HBC units (*26*). For the realization of a nanotubular heterojunction using this self-assembling motif, essential requisites are (i) the formation of a morphologically stabilized seed nanotube and (ii) the design of a second graphene monomer capable of tubularly assembling from the extremely thin facets of the seed nanotube termini. Further issues include how to cope with a high dispersibility of the seed nanotube and a solubility of the second monomer under assembling conditions.

A keen examination, taking into account all the above requisites, led us to HBC derivatives **1** and **2** (*27*) as the monomers for the seed and second nanotubular segment, respectively (Fig. 1). HBC **1** carries two bipyridine (bpy) units, in order for the resulting seed nanotube (Fig. 1A) to be morphologically stabilized by wrapping with a metal-coordination network (Fig. 1 B) (*28*). The charged surface of the resultant seed also merits its homogeneous dispersion by an electrostatic repulsion (*29*). On the other hand, HBC **2** bears four electron-withdrawing fluorine substituents, so it can adhere electronically to the seed termini and self-assemble selectively from their nanotubular facets. When these HBC molecules coassemble stepwise (Fig. 1C), the resultant connecting segments are electronically dissimilar to one another (Fig. 1D).

As a typical example of the preparation of the seed nanotube (**$NT_{1•Cu}$**, Fig. 1B), a 5-ml glass vial containing a tetrahydrofuran (THF) solution (2.0 ml) of HBC **1** (0.5 mg, 1.5×10^{-4} M) was placed in a 50-ml glass vial containing 10 ml of methanol (MeOH) and allowed to stand at 25°C, whereupon a yellow suspension gradually formed. Absorption spectroscopy of the suspension after a 24-hour incubation (fig. S1, A and B, broken curve) showed red-shifted absorption bands at 426 and 459 nm characteristic of *J*-aggregated HBCs (*25*, *26*). Scanning electron microscopy (SEM, fig. S2A) and transmission electron microscopy (TEM, fig. S2B) of an air-dried sample of the suspension allowed for visualizing nanotubes (**NT_1**) with a uniform diameter of 20 nm, although they were heavily bundled (Fig. 1A) just like other HBC nanotubes (*25*, *26*). We investigated the metal-coordination capability of **NT_1** by using Cu^{2+}, because bpy is known to bind to Cu^{2+}, affording a $bpy_2•Cu^{2+}$ complex. As soon as a MeOH solution (1.0 ml) of copper(II) trifluoromethanesulfonate [$Cu(OTf)_2$, 0.5 mg, 1.5×10^{-6} mol; 5.0 equivalents to HBC **1**] was added, the suspension containing bundled **NT_1** became clear, suggesting that Cu^{2+} ions are bound to the surface bpy groups (Fig. 1, A to B) and make the nanotubes (**$NT_{1•Cu}$**) electrostatically repulsive from one another (*29*). When an air-dried sample of **$NT_{1•Cu}$**, isolated by filtration and washed with MeOH to remove free $Cu(OTf)_2$, was subjected to SEM, highly dispersed nanotubes were observed (fig. S3A). Complete coordination of Cu^{2+} with bpy-appended HBC **1** was confirmed by matrix-assisted laser desorption ionization time-of-flight (MALDI-TOF) mass spectrometry of isolated **$NT_{1•Cu}$** (fig. S4); no peaks attributable to metal-free **1** were detected, but those assignable to **1•Cu**, dissociated from **$NT_{1•Cu}$**, were. The metal coordination of **NT_1** did not give rise to any shift of the *J*-aggregate absorption bands (426 and 459 nm; fig. S1B, solid curve). Hence, the π-stacking geometry of the HBC units is intact

[1]Functional Soft Matter Research Group, RIKEN Advanced Science Institute, 2-1 Hirosawa, Wako, Saitama 351-0198, Japan. [2]Department of Chemistry and Biotechnology, School of Engineering, The University of Tokyo, 7-3-1 Hongo, Bunkyo-ku, Tokyo 113-8656, Japan. [3]College of Chemistry, Chemical Engineering and Biotechnology, Donghua University, 2999 North Renmin Road, Songjiang, Shanghai 201620, People's Republic of China. [4]Chemical Resources Laboratory, Tokyo Institute of Technology, 4259 Nagatsuta, Midori-ku, Yokohama 226-8503, Japan. [5]Graduate School of Engineering, Osaka University, 2-1 Yamadaoka, Suita, Osaka 565-0871, Japan.

*To whom correspondence should be addressed. E-mail: fukushima@riken.jp (T.F.); aida@macro.t.u-tokyo.ac.jp (T.A.)

ERRATUM

Post date 23 December 2011

Reports: "Detection of the water reservoir in a forming planetary system" by M. R. Hogerheijde *et al.* (21 October, p. 338). On page 339, the mass of the detected water vapor is incorrectly stated to be 7.3 x 10^{24} g. The correct value is 7.3 x 10^{21} g. The HTML version online has been corrected.